Experimental Investigation of a Jet Impinging on a Ground Plane in Crossflow

J. M. Cimbala,* D. R. Stinebring,† A. L. Treaster,‡ and M. L. Billet§
Pennsylvania State University, Park, Pennsylvania
and
M. M. Walters¶
U.S. Naval Air Development Center, Warminster, Pennsylvania

An experimental investigation has been conducted in a wind tunnel to model the impingement of high-velocity jet exhaust flow on the ground, as encountered by V/STOL aircraft. A constant jet velocity was maintained while varying the wind tunnel crossflow velocity, upstream boundary-layer thickness, and height from the ground to the jet exit plane. The radial wall jet, when interacting with the crossflow, forms an oscillating horseshoe-shaped separation bubble, commonly referred to in the literature as a ground vortex. The streamwise distance of the separation point from the jet impingement point is documented here as a function of the flow parameters and geometry. Flow visualization of the flowfield and two-component laser Doppler velocimeter measurements taken through the separation bubble indicate that the separation bubble is highly unsteady and nonsymmetric. This unsteadiness may be related to shear-layer vortices shed from the lip of the jet. Thickening of the upstream boundary layer on the ground plane caused the wall jet to penetrate further upstream. The addition of a large plate flush-mounted to the jet exit caused the ground vortex to move downstream and also decreased the size of the ground vortex.

Nomenclature

C_p = static pressure coefficient equal to $(p - p_a)/(\frac{1}{2}\ \rho V_\infty^2)$
D_j = inner diameter of jet
h = distance from nozzle exit to ground board
p_a = ambient pressure measured with static pressure tap in the freestream
p_0 = maximum pressure in the impingement region
q_0 = reference dynamic pressure equal to $p_0 - p_a$
q_x = dynamic pressure of the wall jet at position x, $q_x = \frac{1}{2}\ \rho u_m^2$
q_v = dynamic pressure of the freestream, $q_v = \frac{1}{2}\ \rho V_\infty^2$
u_m = maximum velocity in wall jet profile at some x-location
V_j = velocity of jet at nozzle exit
V_0 = reference velocity equal to $(2q_0/\rho)^{1/2}$
V_x = velocity in the x-direction
V_y = velocity in the y-direction
V_∞ = wind-tunnel velocity
x = distance along ground board in direction upstream of jet centerline
x_i = jet impingement point
x_s = ground vortex separation point
x_v = ground vortex center point
y = distance normal to the ground board
δ = boundary layer thickness
λ^* = reference jet-to-crossflow velocity ratio = V_0/V_∞
ρ = density

Received May 19, 1987; revision received Oct. 9, 1987.

*Assistant Professor, Mechanical Engineering.
†Research Assistant, Applied Research Laboratory.
‡Research Associate, Applied Research Laboratory.
§Senior Scientist, Applied Research Laboratory.
¶Research Monitor.

Introduction

THE impingement of high-velocity jet exhaust flow on the ground during vertical take-off and landing (VTOL) or short take-off and landing (STOL) flight results in the formation of a wall jet that flows radially from the point of impingement along the ground surface. The interaction of this wall jet with a freestream results in the formation of a stagnation line and the creation of a separated flow area referred to as a ground vortex in previous literature. The location of this stagnation line is dependent on the freestream-to-jet velocity ratio V_∞/V_j, the injection angle of the jet exhaust into the freestream flow, and the normalized height h/D_j of the jet above the ground plane. Because the constant velocity freestream interacts with a radially distributed wall jet, this stagnation line is generally of the shape of the front half of an ellipse whose major axis is aligned with the freestream flow. The location of the center of the vortex region is somewhat downstream of the stagnation line, and of a similar elliptical shape but at some height above the ground. As with the stagnation line, the location and height of this vortex are dependent on V_∞/V_j and h/D_j. Figure 1 shows top and side view schematic diagrams of the flowfield and also the coordinate system adopted here. When flow conditions are appropriate for its formation, the ground vortex is a major cause of the induced flow on a VTOL or STOL aircraft operating in ground effect and the oscillation of the forces and moments detected in wind-tunnel tests of aircraft models under the influence of this flow.

To analyze the forces and moments induced on aircraft in this flight environment, it is necessary to know the location of this vortex region relative to the aircraft. Only a limited number of previous studies of this flowfield are documented. For example, Abbott[1] obtained the dimensions of the recirculating ground vortex through flow visualization for the case of an impinging jet moving along the ground. He used both single and twin nozzle arrangements, and studied the effects of jet temperature and jet inclination (swivel) as well. He found

that the maximum penetration of the wall jet into the direction of the oncoming flow was at a point where $(q_v/q_x)^{1/2} \approx 0.5$, where q_v is the dynamic pressure of the freestream, and q_x is the dynamic pressure of the wall jet based on the maximum wall jet velocity at a given x-location. In other words, for a cold jet, the jet penetrates upstream to a point where, in a test under stationary conditions, the maximum velocity of the wall jet would be twice the velocity of the freestream. Abbott showed this relationship to hold for a wide range of crossflow-to-jet velocity ratios V_∞/V_j, for nozzles at various inclination angles, for heated and cold jets, and for nozzle-height-to-jet-diameter ratios, h/D_j of 4.0 and 20.0.

Shortly after Abbott's work, Colin and Olivari[2] conducted an experiment that featured a circular jet impinging on a ground board that was mounted at the exit of a large circular open jet test section. Their setup permitted height adjustment over the range $0.5 \le h/D_j \le 4.0$, but most of their detailed measurements were at the fixed value $h/D_j = 4.0$. Their experimental techniques included pressure manometry, surface flow visualization, and measurements of the concentration of gases injected into the jet. These measurements showed the elliptical (horseshoe) shape of the separation line along the ground plane.

Colin and Olivari also derived a semi-empirical dimensionless relationship for the vortex separation point

$$(x_s - x_i)/D_j = 1.03\ (\lambda^*)^{0.9} \qquad (1)$$

The reference velocity V_0 is defined as $(2q_0/\rho)^{1/2}$, where q_0 is the reference dynamic pressure on the wall that corresponds to the dynamic pressure that would be generated by the difference between p_0 and p_a (i.e., $q_0 = p_0 - p_a$). Equation (1) was obtained by assuming that the kinetic energy in the wall jet equals the kinetic energy in the crossflow at the point of separation. The crossflow was assumed to be inviscid (i.e., had no boundary layer along the wall). Their experimental data at $h/D_j = 4.0$ agree well with this prediction over a wide range of the parameter λ^*.

Some more recent experiments by Stewart and Kuhn[3,4] have been conducted in a wind tunnel using several configurations of wing-body models with single and multiple jets exhausting normal to a ground plane. They show a comparison of all previously published data of vortex penetration distance vs velocity ratio. There is a significant amount of scatter in the data, especially from different facilities. Stewart and Kuhn explained the discrepancies as resulting from boundary-layer effects in the oncoming crossflow. In general, it seems that in experiments conducted in wind tunnels (where the boundary-layer thickness δ along the ground wall can be large), the ground vortex penetrates further upstream than for the case of a jet moving along stationary ground into still air (no boundary layer). It was impossible to verify this quantitatively from the published data, however, because in many of the experiments boundary-layer thickness was not measured. Kuhn,[5] using a moving ground plane, has recently verified the importance of boundary-layer thickness on vortex location. Stewart and Kuhn[3,4] also indicated the need to establish not only the location of the ground vortex as it varies with freestream and jet exhaust conditions, but also the characteristics of the flowfield inside the recirculating region.

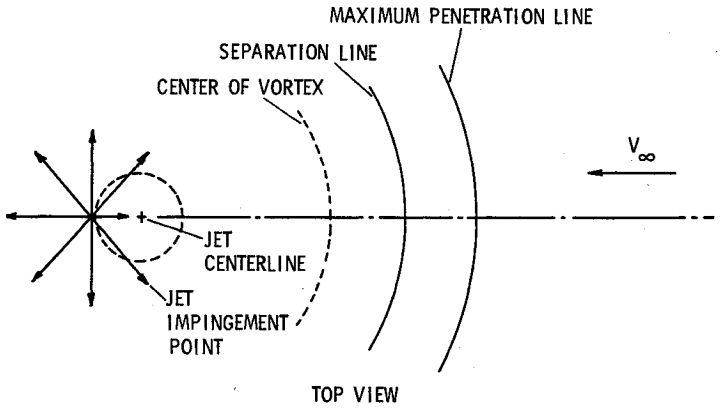

Fig. 1 Ground vortex formed by a jet impinging normally on a flat plate in a crossflow; a) top view, b) side view.

To address this need, an experimental investigation of the formation, stability, and strength of the vortex region was conducted to establish the range of flow conditions that are conducive to development of the vortex. Since detailed, nonobtrusive flow measurements were needed to survey this flow accurately, a two-component laser Doppler velocimeter (LDV) was used to survey the flowfield. Pressure measurements on the ground plane and the smoke-wire flow visualization technique were also used to characterize the flow.

Test Facility and Instrumentation

All tests were conducted in the subsonic wind tunnel at the Applied Research Laboratory of the Pennsylvania State University (ARL-Penn State). This facility is described in detail in Ref. 6. A 76.2-mm-diam round jet was fabricated and inserted through the top of the test section. jet velocity V_j was kept constant at 45.7 m/s, and was powered by a centrifugal blower that injested air from the wind tunnel at a port far downstream from the test chamber. The test chamber was formed by two 2.45-m-long wooden panels, referred to from here on as the ground board and jet board, which spanned the tunnel test section as indicated in Fig. 2. The jet tube extended 152 mm through the jet board at a streamwise distance 1.19 m downstream of its leading edge. The jet board was at a fixed streamwise location, but could be tilted to a positive or negative angle of attack to adjust the pressure gradient between the jet and ground boards. The ground board was attached to inserts along the tunnel walls, and could be positioned 1 to 4 jet diameters from the jet exit plane. The ground board was also equipped with an array of 72 static pressure taps. A Thermal Systems Inc. (TSI) two-component backscatter LDV system was used to survey the region upstream of the jet impingement point along the ground board centerline.

Smoke-wire flow visualization photographs were obtained with a 0.17-mm-diam nichrome wire, stretched vertically through the wind-tunnel walls and held in tension by a spring mechanism. The technique, perfected by Corke et al.,[7] produces streaklines by burning oil droplets on the wire. More details about the experimental setup and instrumentation can be found in Ref 8.

The characteristics of the jet were measured outside of the confines of the wind tunnel. With $V_j = 45.7$ m/s across the jet centerline, mean and fluctuating velocity surveys were conducted up to 6.0 jet diameters axially away from the jet exit. The velocity profile at the jet exit plane was quite flat, with a thin turbulent shear layer along its circumference. Details can be found in Ref. 8. Prior to detailed measurements and flow visualizations of the jet impingement area and ground vortex region, wall-to-wall five-hole probe surveys of the velocity field between the ground board and the jet board were conducted to document the uniformity of the test chamber. It was found that the crossflow velocity V_∞ between the jet board and ground board decreased when the jet was turned on. Apparently, the jet added resistance to the flow and deflected some of the crossflow to the opposite side of the ground board. During the detailed test runs, crossflow velocity was monitored with a pitot-static probe mounted between the ground and jet boards; the resistance effect was thus correctable by simply increasing wind tunnel speed when the jet was turned on.

The five-hole probe surveys through the test chamber and static pressure tap measurements along the ground board with the jet on and off are reported in Ref. 8. In either case (jet on or off), the crossflow velocity was quite uniform with negligibly small transverse velocities.

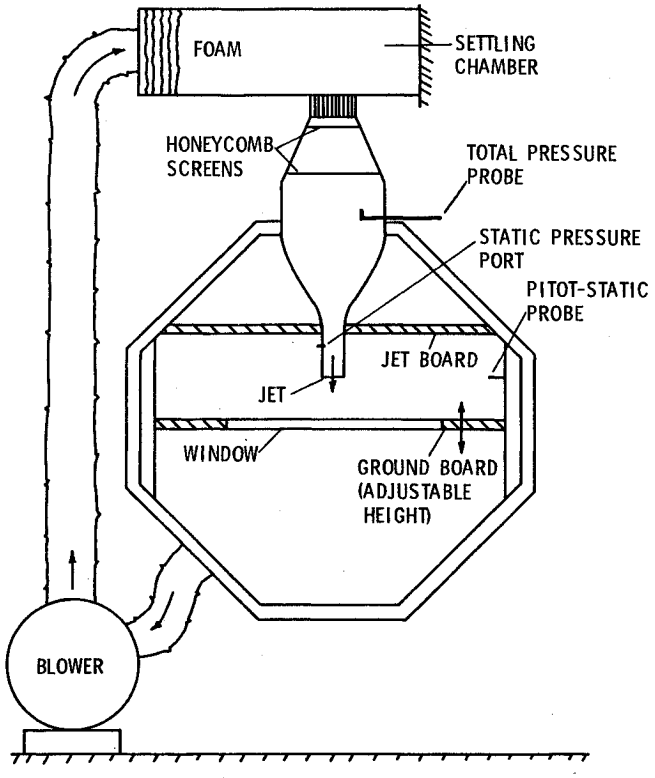

Fig. 2 Schematic of test configuration as installed in wind tunnel (view is from upstream of the test section).

Results

Wall Jet and Bondary Layer

Velocity surveys of the wall jet itself were taken (without crossflow). Figure 3 shows one such survey for $V_j = 45.7$ m/s, $h/D_j = 3.0$, and at a streamwise location 4.8 jet diameters upstream of the jet centerline. For comparison, the semi-empirical wall jet profile, as found in Ref. 2, is also plotted. The agreement is excellent. Velocity surveys of the boundary layer on the ground board were also measured (with the jet off). Three profiles are shown in Fig. 4, and are discussed below.

Flow Visualizations

Smoke-wire photographs taken with single-flash stroboscopic lighting provided instantaneous flow visualizations of the ground vortex. Photographs were taken for various combinations of h/D_j and V_∞/V_j. Some of these photographs are shown in Figs. 5–7. Figure 5 shows the smoke streakline

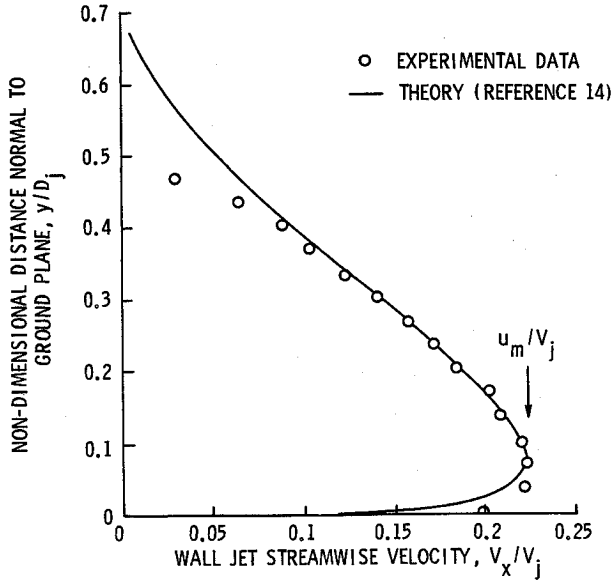

Fig. 3 Wall jet velocity profile at $h/D_j = 3.0$, $x/D_j = 4.8$, with jet velocity $V_j = 150$ ft/s (45.7 m/s) and no crossflow.

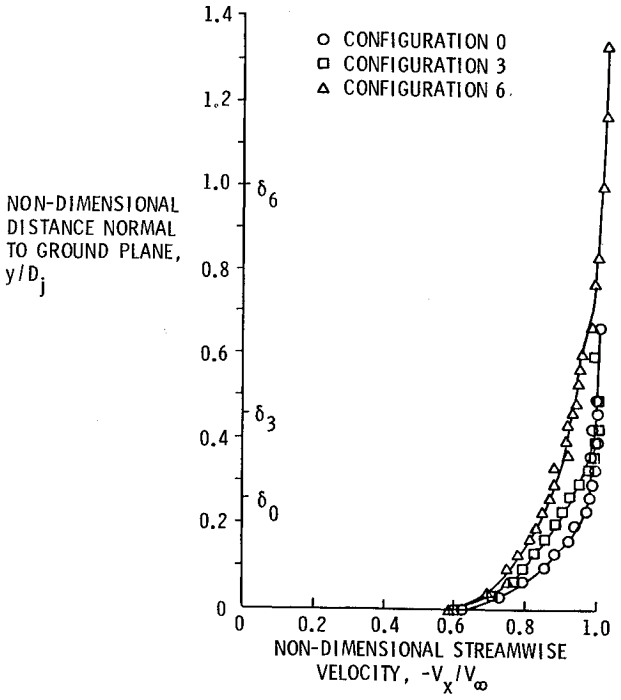

Fig. 4 Boundary-layer profiles at $V_\infty = 30.0$ ft/s (9.14 m/s) for configurations 0, 3, and 6 at $x/D_j = 5.33$, and at $h/D_j = 3.0$.

patterns for $h/D_j = 2.0$. Note that the jet tube protruded two jet diameters down from the jet board and, therefore, the total height between ground and jet boards was 4.0 jet diameters. It is clear that the ground vortex decreases in size and moves further downstream as the crossflow velocity increases. Furthermore, it appears that very little of the freestream fluid enters the ground vortex; the freestream apparently flows over the vortex, much as it would over a solid body obstruction in the flow. As will be discussed below, velocity measurements have shown that the ground vortex is really not a vortex at all, but rather a region of separated recirculating flow. The "ground vortex" is thus more properly referred to as a separation bubble.

Photographs a) and b) of Fig. 5 were taken for identical test chamber conditions, but at different times (about a minute apart). Comparing the two, one can see the unsteadiness in the flow pattern. Both are instantaneous snapshots and, therefore, have "frozen" the motion at one arbitrary point in time. The flowfield captured in photograph a) contains one large separation bubble, whereas that of photograph b) is highly distorted and appears to contain two separation bubbles. Several additional photographs for these same conditions were taken (not shown) and reveal the flowfield to be quite unsteady, particularly at the lower crossflow velocities.

Of particular interest in these photographs is the presence of large-scale shear-layer vortices that are generated at the outer edge of the jet. Some of these shear-layer vortices are visible in photos a), c), and d) of Fig. 5.

Figure 6 shows the separation bubble at $h/D_j = 3.0$. For $V_\infty/V_j = 0.1$, the flow was found to be extremely unsteady, but as the crossflow velocity increased, the unsteadiness was damped. The shear-layer vortices discussed above are most clearly visible in photographs b) and c) of Fig. 6. These large-scale coherent structures appear quite similar to those observed by Brown and Roshko[9] for the case of a two-dimensional mixing layer. However, since the jet is axisymmetric, the eddies are probably more similar to those observed by Yale.[10] The extent to which these vortical structures influence the flowfield is unknown, but it is quite possible that they are a major factor in the observed unsteadiness. The eddies amalgamate rapidly as they decelerate while approaching the

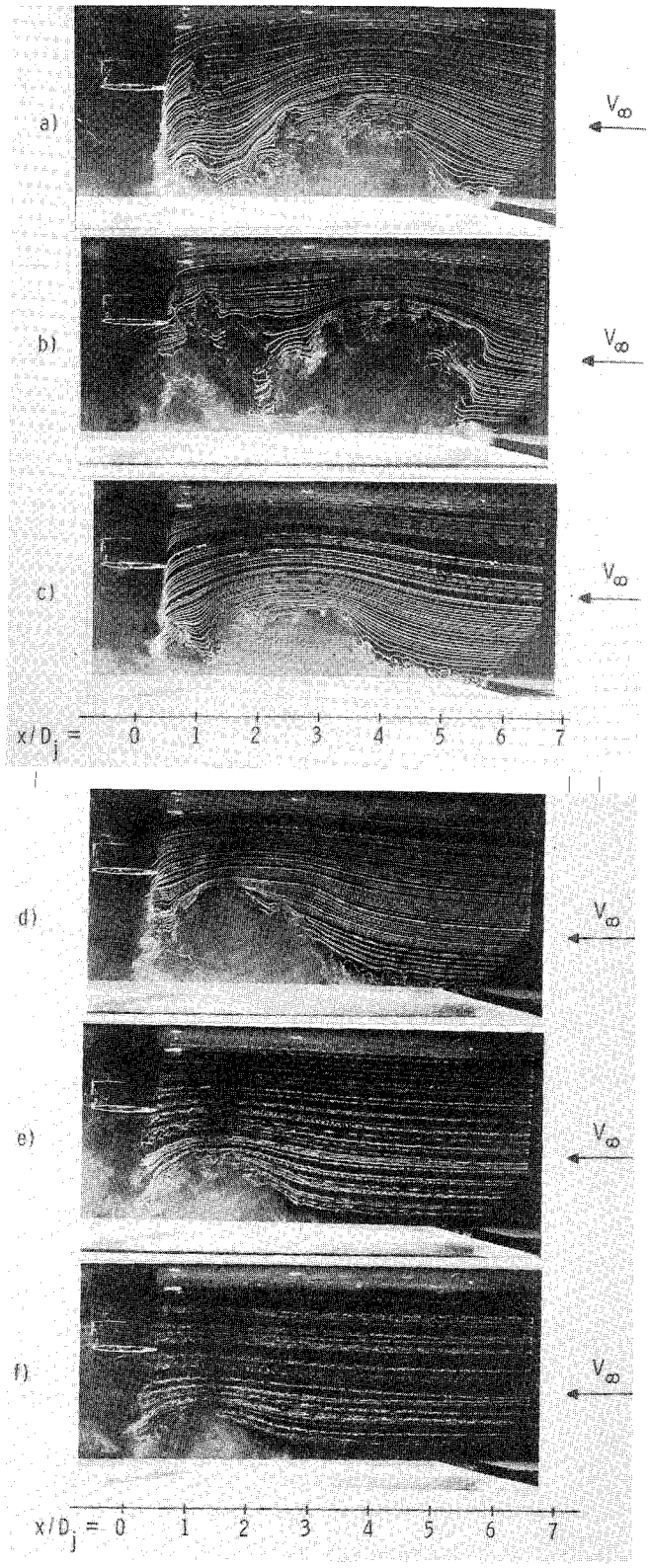

Fig. 5 Smoke-wire photographs of separation bubble for $h/D_j = 2.0$, standard configuration, V_∞/V_j = a) 0.1, b) 0.1, c) 0.15, d) 0.2, e) 0.25, and f) 0.30. [Photos a) and b) are for identical conditions but different times, and illustrate the unsteadiness.]

ground board. The large eddies are then convected upstream with the wall jet, where they interact with vorticity of the same sign associated with the oncoming boundary layer. It is conjected that this results in a large recirculating region which continues to grow until the entire flowfield breaks up, with jet fluid bursting away from the separation bubble. Photograph

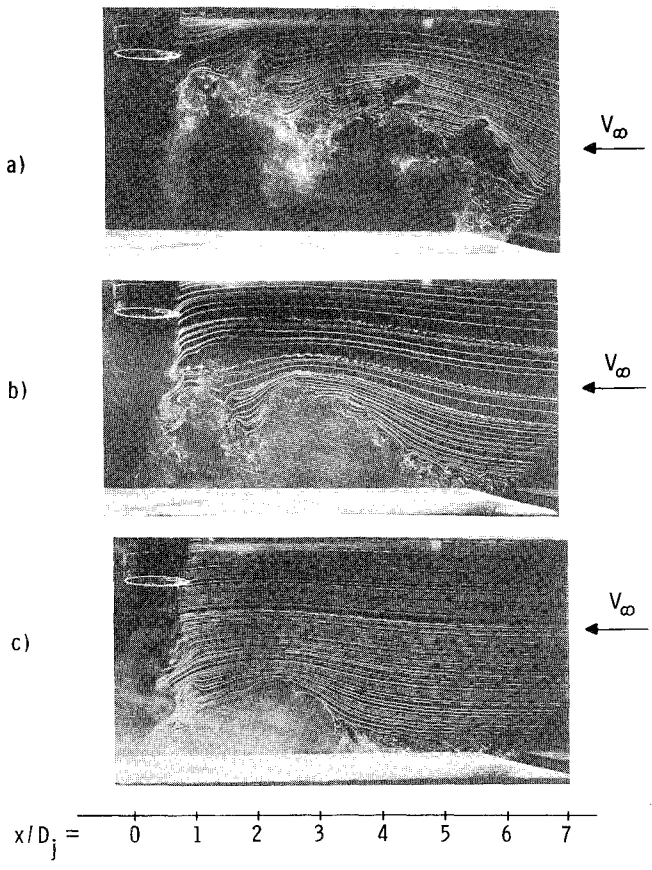

Fig. 6 Smoke-wire photographs of separation bubble for $h/D_j = 3.0$, standard configuration, V_∞/V_j = a) 0.1, b) 0.15, and c) 0.2.

b) of Fig. 5 may be a snapshot of the flowfield just after one of these breakups; the separation bubble here is highly distorted and three-dimensional. The process then repeats itself.

Figure 7 shows the flowfield visualized at $h/D_j = 4.0$. Photograph a) at $V_\infty/V_j = 0.1$ has captured some extremely large shear-layer vortices convecting down from the jet exit plane. This photograph also reveals what appears to be one of the "bursts" discussed above occurring at the top of the separation bubble. Another feature prominent in this series of photographs is the location of the impingement point. Note how, as crossflow velocity increases, the jet is swept downstream and impinges at a point on the ground board further downstream than the jet centerline. At large values of h/D_j, this is more noticeable. In fact, photograph d), at $V_\infty/V_j = 0.3$, shows a case where the cross-flow velocity was so high that it swept the jet completely off of the ground board; no separation bubble can be defined for this case.

We should point out here that the waviness and nonuniformity of the smoke streaklines at the higher velocity cases are not due to any inherent nonuniformities of the freestream flow in the wind tunnel, but rather are due to vortex shedding from the smoke-wire itself. At high freestream velocities, the Reynolds number of the smoke-wire is greater than 40, and is thus unstable to the periodic shedding of vortices. This small-scale structure had negligible influence on the flowfield of interest.

Pressure Distributions

Time-averaged pressure distributions were recorded along the ground board via an array of static pressure taps for several combinations of h/D_j and V_∞/V_j. An example is shown in Fig. 8 for the case $h/D_j = 3.0$, and $V_\infty/V_j = 0.2$. The impingement point x_i of the jet is easily identified as the point of maximum C_p. Moving upstream (left to right in Fig.

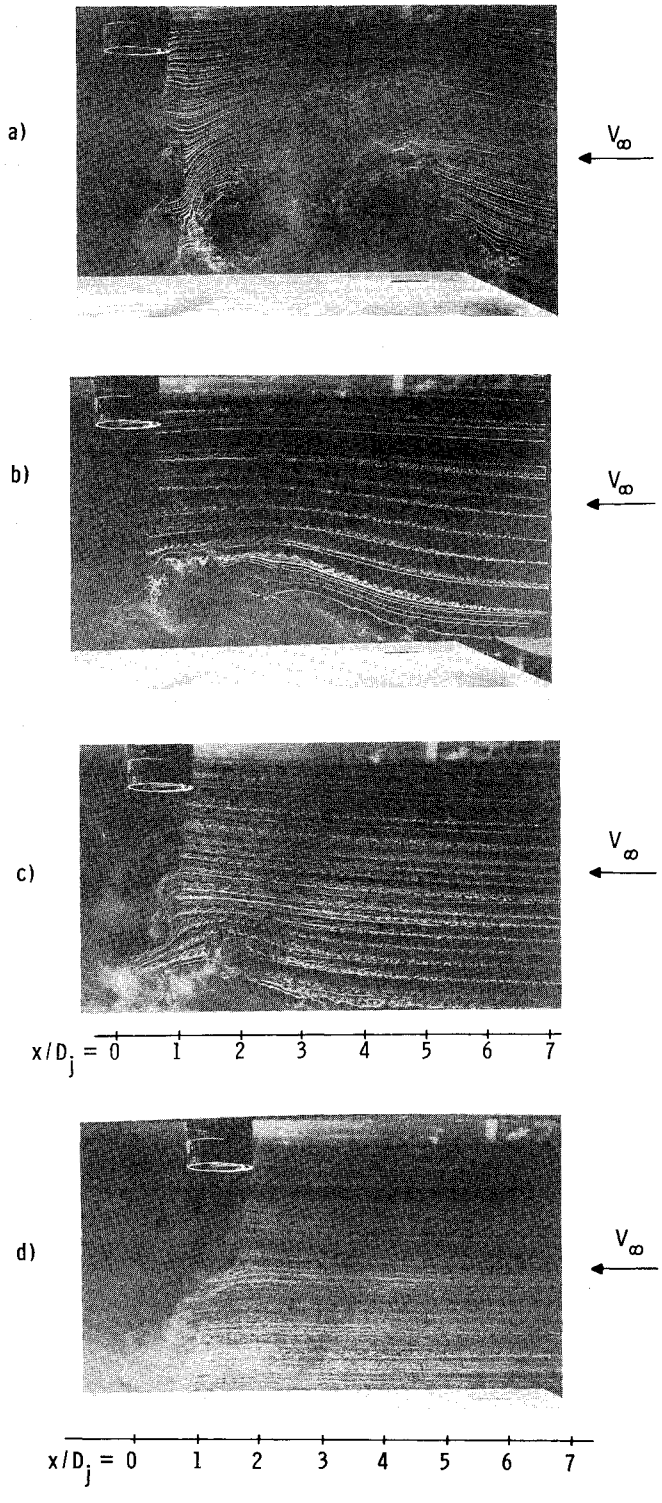

Fig. 7 Smoke-wire photographs of separation bubble for $h/D = 4.0$, standard configuration, V_∞/V_j = a) 0.1, b) 0.15, c) 0.2, and d) 0.3.

8), the pressure coefficient drops to a negative value, rises again above zero, and then slowly returns to zero far upstream. Colin and Olivari[2] have identified the negative C_p region as the approximate location of the ground vortex, with x_v the vortex center at the minimum C_p point. The zero-crossing point has been labeled x_s on Fig. 8, and has been found to correspond to the separation point identified by minituft surface flow visualization.[8] Similar pressure distributions along the centerline of the ground board have been taken for various values of h/D_j and V_∞/V_j. Table 1 shows a list of

impingement point x_i/D_j, separation point $(x_s\text{-}x_i)/D_j$, and vortex location $(x_v\text{-}x_i)/D_j$, as measured from the experimental pressure distributions. Also shown in the table are the maximum C_p (at impingement) and the minimum C_p (at the vortex center). The minimum C_p gives some indication of the strength of the ground vortex.

The trends indicated in Table 1 also agree qualitatively with those of the smoke-wire flow visualizations. Namely, for a fixed jet-to-ground-plane distance h/D_j, the separation bubble moves progressively downstream while decreasing in size and strength as freestream velocity is increased. As expected, the impingement point pressure decreases as h/D_j increases for the same velocity ratio, since the jet is further from the ground board and has more time to dissipate before impingement. The impingement point itself moves downstream as h/D_j or V_∞/V_j is increased, which agrees with the flow visualization results discussed above.

Effect of Upstream Boundary-Layer Thickness

One important aspect of this problem has been neglected in most of the previous work, namely, the effect of the thickness of the oncoming boundary layer. The current experimental setup permitted artificial thickening of the boundary layer on the ground board upstream of the region of interest. A combination of sandpaper roughness and a trip wire resulted in normalized boundary-layer thickness δ/D_j ranging from 0.27 to 1.00. Details of the configuration geometries can be found in Ref. 8. Figure 4 shows the boundary-layer profiles for three of these configurations. (Configuration 0 is the case with no roughness added, and had the smallest boundary layer. Configurations 3 and 6 refer to an intermediate and thick boundary layer, respectively.) These boundary-layer surveys were conducted for $h/D_j = 3.0$ at a streamwise distance of $x/D_j = 5.33$, which is 787 mm downstream of the ground board leading edge. These surveys were conducted with the jet off and at a freestream velocity of 9.14 m/s.

As the boundary layer thickens, the wall jet encounters less resistance near the wall; therefore, the jet should be able to penetrate further upstream. Smoke-wire photographs of the three configurations are shown in Fig. 9. As expected, the ground vortex appears to move upstream as boundary-layer thickness is increased. In Fig. 9c, the small-scale turbulent structure in the thick boundary layer is clearly visible; in this case, it is quite difficult to identify the leading edge of the separation bubble. Some similar results have been obtained very recently by Kuhn[5] for the ground vortex formed in a water channel. For the thick boundary-layer case, Kuhn refers to the region just upstream of the separation point as a "boundary layer wedge." He suggests the possibility that vortices in this wedge may contribute to the unsteadiness observed in the flowfield.

A quantitative comparison was also made using the static pressure taps along the centerline of the ground board. Figure 8 shows the static pressure coefficient distribution for configurations 0 and 6, at $V_\infty/V_j = 0.2$ and $h/D_j = 3.0$. Note that separation point $(x_s - x_i)/D_j$ changes from 2.90 to 3.23, respectively, as δ/D_j increases from 0.27 to 1.0. This represents a percentage change in separation point of only 11% for a change in boundary-layer thickness of over 270%.

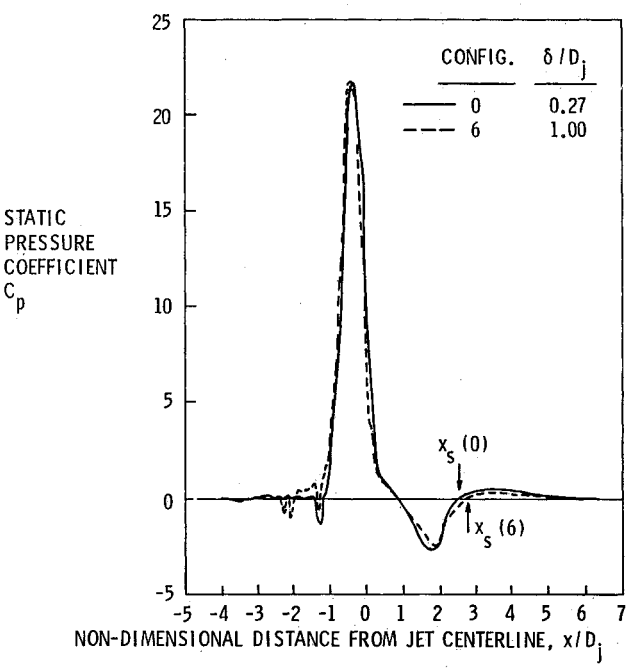

Fig. 8 Comparison of static pressure distribution along centerline of ground plane for $h/D_j = 3.0$ and $V_\infty/V_j = 0.2$ for configurations 0 and 6.

Effect of Flush-Mounted Jet Plate

All of the previous results have been for what will be called the "standard configuration," where the jet tube protruded 2.0 jet diameters away from the jet board in order to eliminate any boundary-layer effects of the upper wall on the jet flow. Tests were also conducted with a modified configuration, where a large jet plate was installed between the jet and ground boards with its lower surface flush-mounted with the jet exit plane. This was done to simulate the more realistic case of jet exhaust from the underbelly of a V/STOL aircraft wing. The jet plate consisted of a 457.2 × 457.2 mm area, 19.1-mm-thick plate with a rounded leading edge. The jet was located in the center of this plate, and the ratio of the plate area to the jet exit area was 45.8.

Smoke-wire photographs were taken of the test chamber with and without the jet plate added, for $h/D_j = 3.0$ and $V_\infty/V_j = 0.1$, 0.15, and 0.2, as shown in Fig. 10. Compared to Fig. 6 (standard configuration without a jet plate), it appears that the jet plate causes the separation bubble to decrease significantly in size; the separation point also moves further downstream. A quantitative comparison of the two configurations at $h/D_j = 3.0$ and $V_\infty/V_j = 0.2$ is shown in Fig. 11 where static pressure distributions on the centerline of the ground plane are plotted. The separation point $(x_s - x_i)/D_j$ decreased about 20%, i.e., from 2.9 to 2.3 with the addition of the jet plate. Not only does the separation bubble decrease in size and move downstream when the jet plate is added, but $C_{p_{max}}$ (at

Table 1 Ground vortex characteristics as determined from surface pressure distributions

h/D_j	V_∞/V_j	x_i/D_j	$(x_s - x_i)/D_j$	$(x_{mp} - x_i)/D_j$	$C_{p_{max}}$	$C_{p_{min}}$
1.0	0.10	−0.07	4.63	3.37	107.9	−7.56
1.0	0.15	−0.13	3.57	2.80	45.9	−5.20
1.0	0.20	−0.13	2.87	2.33	25.7	−4.33
1.0	0.30	−0.10	2.10	1.73	10.7	−3.24
1.0	0.40	−0.07	1.50	1.27	5.7	−2.07
2.0	0.10	−0.10	5.18	3.63	106.5	−6.22
2.0	0.15	−0.16	3.83	2.83	45.2	−4.33
2.0	0.20	−0.23	3.03	2.37	25.2	−3.54
2.0	0.30	−0.33	1.80	1.46	9.8	−2.00
2.0	0.40	−0.83	****[a]	****[a]	3.1	****[a]
3.0	0.10	−0.17	5.87	4.13	103.0	−5.00
3.0	0.15	−0.23	4.23	2.86	44.5	−3.54
3.0	0.20	−0.33	2.90	2.10	21.5	−2.81
3.0	0.30	−1.13	1.30	0.10	4.6	−0.18
4.0	0.10	−0.27	6.03	4.20	90.9	−4.25
4.0	0.15	−0.47	3.80	2.80	35.0	−3.15
4.0	0.20	−0.83	2.33	1.93	12.5	−2.07

****[a] indicates ground vortex not identifiable from pressure distribution.

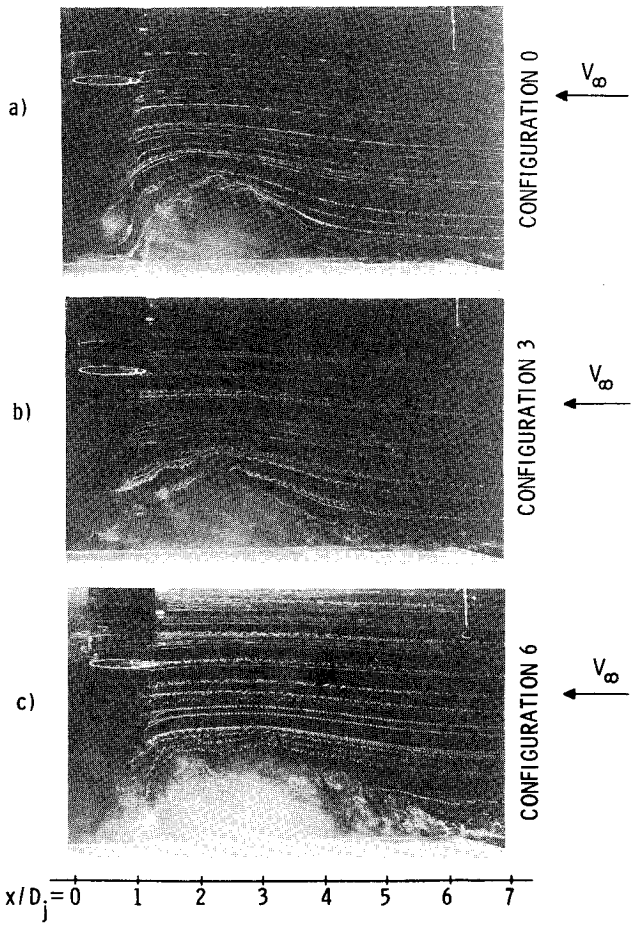

Fig. 9 Effect of boundary-layer thickness on separation bubble size and shape, $h/D_j = 3.0$, $V_\infty/V_j = 0.2$, δ/D_j = a) 0.27 (20 mm), b) 0.37 (28 mm), and c) 1.0 (76 mm).

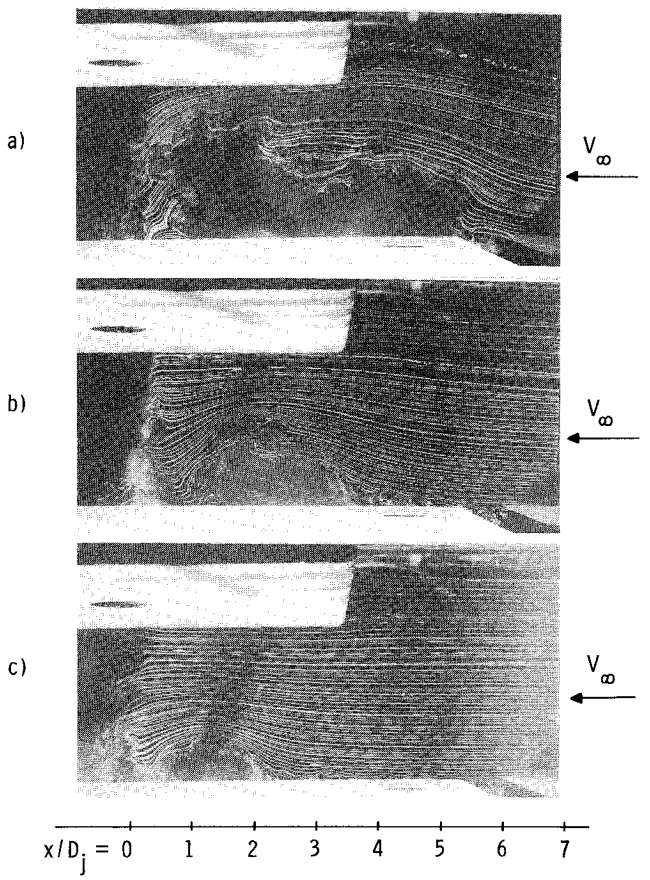

Fig. 10 Effect of jet plate flush-mounted on jet exit plane at zero angle of attack, $h/D_j = 3.0$, V_∞/V_j = a) 0.1, b) 0.15, and c) 0.2.

the jet impingement point) decreases as well. There are at least three possible explanations for these observations. First, with the jet plate added, there is a boundary layer at the jet exit plane, which may affect the jet characteristics. Second, the jet plate adds blockage to the flow. in the test chamber; since the freestream velocity and pressure were monitored upstream of the jet plate, the velocity between the jet plate and ground board would be somewhat higher. Higher freestream velocity, as discussed above, pushes the separation bubble downstream and decreases $C_{p_{max}}$ Finally, and perhaps most significantly, with the addition of the jet plate there is a reduction in height between the ground board and the upper wall, which restricts the vertical size of the separation bubble. In other words, the separation bubble does not have room to grow in height and is, therefore, weakened and pushed downstream. No attempt has been made here to analyze these effects separately.

Laser Doppler Velocimeter Measurements

LDV flow measurements were taken for several of the configrations; Fig. 12 shows the results for $h/D_j = 3.0$ and $V_\infty/V_j = 0.2$ in the form of a time-averaged velocity vector plot. The vector plot of the velocity field provides a visualization of the mean flow in the vicinity of the ground vortex. For all cases the cross section through the vortex has an elliptical shape. Furthermore, the velocity profile through the center of the vortex is not at all like that of a Rankine-type vortex. This is the reason that ground vortex is somewhat of a misnomer; "rotating separation bubble" is perhaps a more appropriate designation for the flowfield observed here. Reference 8 includes more details about the LDV surveys, including velocity probability histograms that give some quantitative information about the unsteadiness discussed above.

Discussion

Results have been presented for ground vortex size, shape, and location as a function of jet-to-ground-board height h/D_j, crossflow-to-jet velocity ratio V_∞/V_j, and oncoming boundary-layer thickness δ. These data will now be compared to those of other experiments. The separation distance $(x_s - x_i)/D_j$ is the parameter most readily compared, since it can be determined either from surface flow visualization or from static pressure measurements along the ground board. Colin and Olivari[2] appear to have been the first to attempt to predict the location of the separation point with a kinetic energy flux matching scheme. Assuming a zero-thickness (inviscid) oncoming boundary layer and a semi-empirical equation for the wall-jet velocity profile, they developed the prediction given by Eq. (1). Their experimental data at $h/D_j = 4.0$ agree well with this prediction over a wide range of the parameter λ^*.

It can be shown that the reference-jet-to-crossflow velocity ratio λ^* is equivalent to the square root of $C_{p_{max}}$ at the jet impingement point:

$$\lambda^* = \frac{V_0}{V_\infty} = \frac{(2q_0/\rho)^{1/2}}{V_\infty} = \left(\frac{p_0 - p_a}{\frac{1}{2}\rho V_\infty^2}\right)^{1/2} = (C_{p_{max}})^{1/2} \qquad (2)$$

The values of $(x_s - x_i)/D_j$ from the current static pressure distribution measurements are plotted in Fig. 13 as a function of λ^*. The results from Eq. (1) are also shown for comparison.

Although parameter λ^* appears to adequately collapse the data for various combinations of h/D_j and V_∞/V_j, the current experimental data fall well below the predicted curve and experiments of Colin and Olivari. In general, it appears that

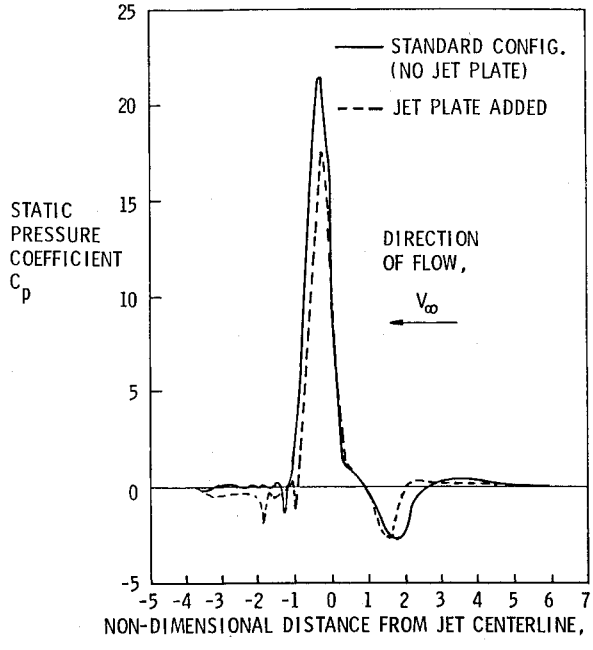

Fig. 11 Static pressure distribution along centerline of ground plane for $h/D_j = 3.0$, $V_\infty/V_j = 0.2$ with and without flush-mounted jet plate.

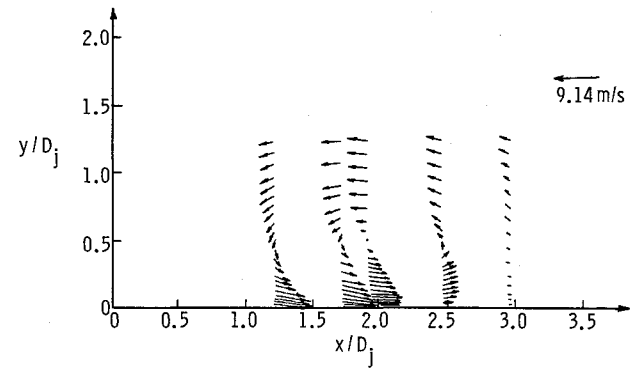

Fig. 12 Vector plot of velocity field for $V_\infty/V_j = 0.2$ and $h/D_j = 3.0$.

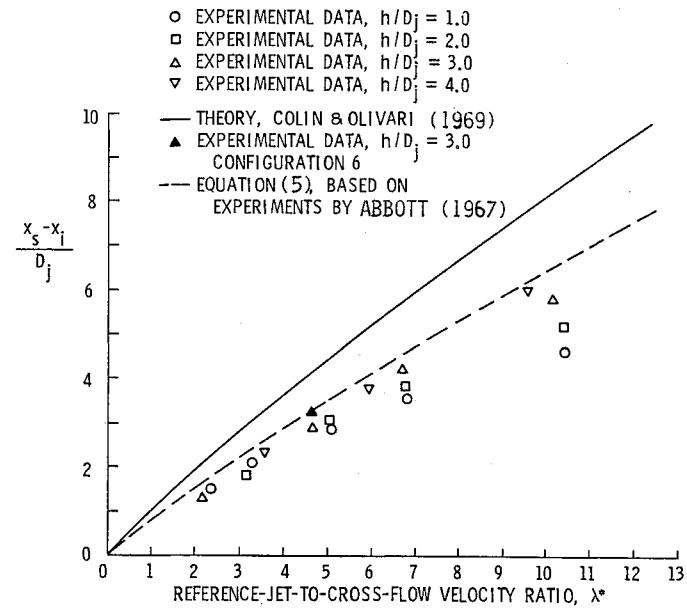

Fig. 13 Comparison of experimental and theoretical locations of separation points x_s for various values of h/D_j.

the data at higher values of h/D_j are closer to the prediction than those for low values of h/D_j.

There are several plausible explanations for the disagreement between Eq. (1) and the present results. Colin and Olivari's theory neglects boundary-layer thickness. However, a thick boundary layer has lower momentum or kinetic energy flux and, therefore, allows the wall jet to penetrate further upstream. Thicker boundary layers would, therefore, shift Colin and Olivari's curve even higher, and the current data would be further away from the theory. The solid triangle in Fig. 13 represents one experimentally measured value of separation point for configuration 6 (the configuration with the maximum boundary-layer thickness generated in the current study at $h/D_j = 3.0$ and $V_\infty/V_j = 0.2$). As noted above, although δ was increased by over 270%, the normalized separation distance increased only by about 11%. Colin and Olivari give no boundary-layer thickness measurements in their report, but based on their geometry and velocities, δ is probably about the same order of magnitude as the current configuration 0 case. Thus, boundary-layer effects alone are not sufficient to explain the discrepancy between the two experiments.

Some interesting results have been obtained recently (concurrent with the present research) in a water tunnel by Kuhn,[5] who measured separation point with and without motion of an endless belt ground plane. With the ground belt moving at V_∞, the separation point moved downstream by as much as 40 or 50%, compared with the case of a stationary ground plane. This illustrates the importance of the boundary condition imposed on the flowfield. Namely, results for a jet moving along the ground in still air are much different from those for the same jet fixed in a freestream above stationary ground. In the former case, relative to coordinates fixed on the jet, the ground plane underneath the radially spreading wall jet provides a strong shear in the direction opposing the wall jet due to the no-slip condition. In the latter case (jet and ground fixed in a crossflow), this opposing shear stress is much smaller. Both the present investigation and that of Colin and Olivari[2] were of the latter type.

Another possible contributor to the discrepancy in Fig. 13 is differences in the characteristics of the jets themselves. Mean and fluctuating velocity profiles for the present jet are documented in Ref. 8. Colin and Olivari used a 50.0 mm jet, but unfortunately did not document either V_j or V_∞. Their detailed measurements were conducted at $h/D_j = 4.0$, but normalized mean velocity profiles for their jet were reported only to 1.64 jet diameters from the jet exit; fluctuating velocities were not reported. Direct comparison of the two jets was, therefore, not possible even though both jets were run with air at ambient temperature. As discussed above, the characteristics of the jet (such as turbulence intensity and the existence of large-scale vortical structures) are believed to be quite important, particularly with respect to the unsteady features of the separation bubble.

Perhaps the most significant single factor that distinguished the present experiments from those of Colin and Olivari is the presence of an upper wall, referred to here as the jet board. The present experiments were conducted in a closed, recirculating wind tunnel with two large boards mounted parallel to the flow—the ground board and the jet board. The total available height between the two boards for formation of the ground vortex ranged from 3.0 to 6.0 jet diameters. On the other hand, Colin and Olivari conducted their tests in a large open jet facility with no upper wall. Their flow was, therefore, not as restricted with respect to vertical growth as the present flow. In the absence of a restricting upper wall, the ground vortex would be expected to move upstream and increase in size. This is exactly the trend found in comparing the present data to those of Colin and Olivari.[2] It has been shown by Stewart and Kuhn[3] that the presence of a jet plate has

significant influence on ground vortex size, location, and strength. In particular for jet plate heights below about four jet diameters, Stewart and Kuhn show an aft movement of the ground vortex, when compared to the case without an upper jet plate. Apparently, the geometrical restrictions imposed on vertical growth of the ground vortex lead to a "trapped vortex" phenomenon below some critical height. Tests in the present facility with and without an additional flush-mounted jet plate confirm the finding of Stewart and Kuhn. Namely, significant downstream movement of the ground vortex was found when a jet plate was flush-mounted to the jet exit.

In a separate experiment, Abbott[1] studied the case of a moving jet impinging on stationary ground. His data collapse universally to the simple expression that for a cold jet, the wall jet penetrates upstream to a point where, under stationary conditions, the maximum velocity of the wall jet would be approximately twice that of the oncoming freestream:

$$\frac{u_m}{V_\infty} \approx 2.0 \tag{3}$$

By definition, $\lambda^* = V_0/V_\infty$. The maximum wall jet velocity u_m is related to jet reference velocity V_0 by

$$\frac{u_m}{V_0} = 1.56 \left(\frac{x - x_i}{D_j}\right)^{-1.1} \tag{4}$$

according to the semi-empirical stationary wall jet calculations found in Colin and Olivari.[2] Combining Eqs. (3) and (4) one obtains for separation point x_s

$$\frac{x_s - x_i}{D_j} = 0.80\ (\lambda^*)^{0.91} \tag{5}$$

which is shown as the dashed line in Fig. 13. As seen, the present experimental data compare much better to this curve than to the one above it, although the experimental points still lie below the curve. Since there was no upper restricting wall in Abbott's experiments, one would expect the separation point under these conditions to occur somewhat further upstream when compared to data taken in a closed wind tunnel. Notice that as height h/D_j increases, the data agree more closely with Abbott's curve. Note, however, that Abbott's experiments were conducted with the jet moving along stationary ground, which corresponds to Kuhn's moving belt experiment.[5] Thus, the effect of ground boundary conditions must also be considered when comparing the present results with those of Abbott, as discussed above. It is not possible to separate the effects of boundary-layer thickness, ground boundary conditions, jet characteristics, or upper wall effects in these comparisons with other experiments.

The most interesting aspect of the present experiments is the relationship between observed unsteadiness in the flowfield and large-scale vortical structures shed from the lip of the jet. The flow visualizations reported here indicate that these vortical structures amalgamate into a large recirculating separation bubble, which is continually fed by both the shear layer vortices from the jet and the vorticity from the oncoming boundary layer. It is conjected that this separation bubble grows until it can no longer be sustained; total breakdown of the symmetry of the separation bubble seems to result, and then the process presumably repeats itself. Further experiments are required to verify this conjecture.

Conclusions

In summary, the rotating separation bubble formed by an impinging jet in a crossflow has been studied experimentally. The bubble was found to move downstream and decrease in size and shape as freestream-to-jet velocity ratio V_∞/V_j was increased. Artificial thickening of the oncoming boundary layer resulted in further upstream penetration of the wall jet, but this factor alone is not sufficient to account for the large scatter in data from various facilities. The addition of a flush-mounted jet plate led to significantly less upstream penetration of the ground vortex. Further experimentation is required to determine the effects of jet characteristics (such as turbulence intensity and the presence of large-scale vortical structures), upper wall restrictions, and ground plane motion.

Acknowledgements

This program was funded by The U.S. Naval Air Development Center, Warminster, Pennsylvania. The authors acknowledge the experimental assistance of T. J. Davis, D. P. Mrozinski, and C. M. Zakrowzki during the investigation.

References

[1]Abbott, W. A., "Studies of Flow Fields Created by Vertical and Inclined Jet When Stationary or Moving Over a Horizontal Surface," Ministry of Aviation, Aeronautical Research Council, London, Great Britain, CP No. 911, 1967.

[2]Colin, P. E. and Olivari, D., "The Impingement of a Circular Jet Normal to a Flat Surface With and Without a Cross Flow," von Kármán Institute Final Technical Report, U.S. Defense Technical Information Center TR AD688953, Alexandria, VA, Jan. 1969.

[3]Stewart, V. R. and Kuhn, R. E., "A Method for Estimating the Propulsion Induced Aerodynamics Characteristics of STOL Aircraft in Ground Effect," Naval Air Development Center Rept. 80226-60, Aug. 1983; AIAA Paper 83-2494, Oct. 1983.

[4]Kuhn, R. E., "V/STOL and STOL Ground Effects and Testing Techniques," Task I Report, Contract No. NAS2-11912, NASA Ames Research Center, Moffett Field, CA, Dec. 1984.

[5]Kuhn, R. E., "Ground Vortex Investigation in NASA Ames/Dryden Water Tunnel," Private Communication, Nov. 1986.

[6]Parkin, B. R. and Henderson, R. E., "Garfield Thomas Water Tunnel Test Facilities," Applied Research Lab., Pennsylvania State Univ., University Park, PA, Jan. 1980.

[7]Corke, T., Koga, D., Drubka, R., and Nagib, H., "A New Technique for Introducing Controlled Sheets of Streaklines in Wind Tunnels," IEEE Publication 77-CH-1977; 1251-9, 1977.

[8]Cimbala, J. M., Stinebring, D. R., Treaster, A. L., and Billet, M. L., "Experimental Investigation of a Jet Impinging On a Ground Plane in the Presence of a Cross Flow," Report to Naval Development Center, Applied Research Lab., Pennsylvania State Univ., University Park, PA, Feb. 1987.

[9]Brown, G. and Roshko, A. "On Density Effects and Large Structures in Turbulent Mixing Layers," *Journal of Fluid Mechanics*, Vol. 64, 1974, pp. 775–816.

[10]Yule, A. J., "Large-Scale Structure in the Mixing Layer of a Round Jet," *Journal of Fluid Mechanics*, Vol. 89, 1978, pp. 413–432.